Characterization of Transmission Lines with Nonlinear Dielectric Materials

Aaron M. Hagerstrom*, Eric Marksz*†, Christian J. Long*, James C. Booth*, Nathan D. Orloff*
*National Institute of Standards and Technology †University of Maryland

***Abstract*—Nonlinear transmission lines are interesting for several device applications including harmonic generators, and phase shifters. They are also good candidates for characterizing nonlinear materials at mm-wave frequencies. Regardless of the application, circuit modeling is challenging because nonlinear waveguides are described by a nonlinear wave equation. In this paper, we focus on characterizing the nonlinear mixing products generated by coplanar waveguides on a nonlinear ferroelectric $\mathrm{Ba_{0.5}Sr_{0.5}TiO_3}$ (BST) film. We developed a perturbative solution to the nonlinear wave equation, and validate our model by using a nonlinear vector network analyzer (NVNA) to measure the nonlinear mixing products. Our approach is useful for predicting spurious signals generated by nonlinear mixing in devices with nonlinear dielectrics, and predicting the performance of nonlinear devices such as harmonic generators.**

***Index Terms*—Materials characterization, nonlinear vector network analysis, On-wafer metrology, tunable dielectrics**

I. Introduction

Some examples of devices employing nonlinear transmission lines include broadband phase shifters [1], 3rd harmonic generators [2], and non-reciprocal, non-magnetic receiver front-ends [3]. Generally speaking, there are two common ways of creating a nonlinear distributed capacitance: periodically loading a transmission line with tunable capacitors (either varactor diodes or nonlinear dielectric capacitors), and depositing the waveguide on a nonlinear dielectric material. In each case, the nonlinearity is described by a voltage-dependent capacitance and conductance. The same nonlinear wave equation will apply. We focus on nonlinear dielectrics, because dielectric nonlinearity is an important consideration for filters and phase shifters, and because the literature on nonlinear dielectric characterization at mm-wave frequencies is scarce.

Tunable dielectric materials are an attractive solution for frequency-agile microwave components because their permittivity can be tuned by an applied electric field. This field-tunability can be used to build voltage-tunable filters and phase shifters [4]. In a nonlinear material, the field-tunability can be described by modeling the displacement field D as a power series in the electric field E:

$$D \sim \varepsilon^{(1)}E + \varepsilon^{(2)}E^2 + \varepsilon^{(3)}E^3 + \cdots . \tag{1}$$

The linear permittivity $\varepsilon^{(1)}$ is well-known to be strongly frequency-dependent in the 10's of GHz for many materials of interest [5]. With a few notable exceptions [6], dielectric relaxation is a major limitation in many applications. For this reason, we need to understand the frequency dependence of any nonlinear dielectric in a particular circuit design in order to predict that circuit's performance. Dielectric characterization is often performed in an on-wafer environment because it is difficult to fabricate many materials of interest in bulk, and because the eventual application requires on-wafer devices.

The nonlinear permittivity $\varepsilon^{(n>1)}$ is also frequency-dependent. In the ferroelectric literature, measurements of the dispersion $\varepsilon^{(3)}$ at low frequencies ($<$1 GHz) are common. For example, Glazouov and Tagansev used nonlinear measurements to distinguish between different thermodynamic models of a relaxor ferroelectric [7]. $\varepsilon^{(2)}$ and $\varepsilon^{(3)}$ are also routinely measured at optical frequencies, where $\varepsilon^{(2)}$ describes 3-wave mixing, 2nd-harmonic generation, optical rectification, the electro-optic effect, and many other phenomena, while $\varepsilon^{(3)}$ describes 3rd order phenomena including 4-wave mixing, self-phase modulation, and 3rd-harmonic generation.

In the 10's of GHz, nonlinear permittivity characterization is difficult, especially in an on-wafer environment. At low frequencies, we can use capacitors, and measure current and voltage directly. At optical frequencies, nonlinear crystals are often large compared to the wavelength of light, and nonlinear mixing can be analyzed by the slowly-varying envelope approximation. At 10's of GHz, the wavelength of light and the size of the device are both on the order of millimeters, so a fully-distributed description is necessary.

Although nonlinear permittivity characterization is difficult, it is also necessary for accurate circuit modeling. For filters and phase shifters, nonlinear mixing products are viewed as spurious signals that degrade performance. For soliton generators, harmonic generators, and non-reciprocal non-magnetic front-ends, nonlinear frequency mixing is the goal of the device. In either case, we needs to know the nonlinear permittivity to accurately predict nonlinear mixing products.

In this paper, we provide an analytic description of frequency mixing in a waveguide with nonlinear distributed admittance per unit length. Much of the previous work on nonlinear dielectric transmission lines focuses on 3rd-order nonlinear effects, which are dominant when the sample is not poled by an external electric field [8], [9]. In contrast, we apply a DC electric field, and observe 2nd-order effects. Since we are focusing on a 2nd-order nonlinearity, we had to develop a new analytical solution. From a mathematical perspective, the techniques we apply are well-known [10], [11], but we have yet to see our solution to this nonlinear problem elsewhere in the literature, and our solution appears to be easy to implement numerically and accurate. For these reasons, we feel that it is of interest to the measurement community.

978-1-5386-4356-3/17/$31.00 ©2017 IEEE

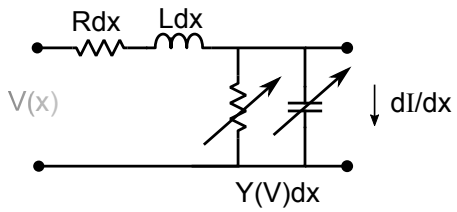

Fig. 1: Conceptual picture of an infinitesimal section of a nonlinear transmission line.

We compare these theoretical predictions to wave parameter measurements of transmission lines that are lithographically patterned on a BST sample. We also discuss the discuss the extraction of $Y^{(2)}$, the strength of the distributed circuit nonlinearity, and $\varepsilon^{(2)}$, the material nonlinearity, from measurements.

II. Formulation

In this section, we derive a model for the nonlinear waves generated by the mixing of two incident sinusoidal signals in a nonlinear transmission line. Figure 1 shows a conceptual picture of an infinitesimal section of transmission line dx with an nonlinear distributed capacitance $C(V)$ and conductance $G(V)$. We lump these two parameters into a distributed admittance $Y(V) = j\omega C(V) + G(V)$. We expect that the admittance will have a similar power series expansion to Equation (1):

$$\frac{dI}{dx} - \sim Y(V)V \sim -Y^{(1)}V - Y^{(2)}V^2 + ... \tag{2}$$

We will focus on 2nd-order nonlinearities, which means we will include $Y^{(1)}$ and $Y^{(2)}$ in our model, but not higher terms. These parameters are both frequency-dependent, because we expect that they are linearly related to $\varepsilon^{(1)}$ and $\varepsilon^{(2)}$.

We consider the case where the waveguide is excited by two waves with angular frequencies ω_1 and ω_2. These waves will generate nonlinear mixing products at $\omega_1 + \omega_2$, $\omega_1 - \omega_2$, $2\omega_1$ and $2\omega_2$. The voltage in the transmission line, as a function of position and time, can be decomposed into components that vary sinusoidally in time:

$$\begin{aligned} V(x,t) = &\hat{V}_1(x)\exp\left[j\omega_1 t\right] + \\ &\hat{V}_2(x)\exp\left[j\omega_2 t\right] + \\ &\hat{V}_{1+2}(x)\exp\left[j\left(\omega_1+\omega_2\right)t\right] + \\ &\hat{V}_{1-2}(x)\exp\left[j\left(\omega_1-\omega_2\right)t\right] + \\ &\hat{V}_{2\times1}(x)\exp\left[j\left(2\omega_1\right)t\right] + \\ &\hat{V}_{2\times2}(x)\exp\left[j\left(2\omega_1\right)t\right] + c.c. \end{aligned} \tag{3}$$

Here, $c.c.$ denotes complex conjugate of all of the terms that are written explicitly in Equation (3). A similar expansion can be written for the current. We will use subscripts to denote frequency. $\hat{V}_1(x)$ is the voltage wave with frequency ω_1 , $\hat{V}_{1+2}$ has a frequency of $\omega_1+\omega_2$, $\hat{V}_{2\times1}$ has a frequency of $2\omega_1$, and so on.

This model assumes small signal amplitudes. The meaning of "small" depends on context. The permittivity of our BST sample tuned by a factor of 2 with a bias voltage of 13.5 V, so we expect that signals with an amplitude on the order of 100 mV are still small. Small signals allow for two simplifying assumptions in our model: first, as we have already stated, we will ignore mixing products beyond the 2nd order. Second, we will assume that $\hat{V}_1, \hat{V}_2 >> \hat{V}_{1+2}, \hat{V}_{1-2}, \hat{V}_{2\times1}, \hat{V}_{2\times2}$, which will allow us to ignore the nonlinearity when solving for the voltage and current waves associated with the incident tones. This is called the undepleted pump approximation in nonlinear optics.

A. Nonlinear wave equations

Under the assumption that the incident tones are much larger than the nonlinear mixing products, the voltage and current waves are given by:

$$\frac{d\hat{I}_i}{dx} \approx -Y^{(1)}(\omega_i)\hat{V}_i \tag{4}$$

$$\frac{d\hat{V}_i}{dx} \approx -\left[R(\omega_i) + j\omega_i L(\omega_i)\right]\hat{I}_i, \tag{5}$$

where $R(\omega_i)$ and $L(\omega_i)$ are the distributed resistance and inductance per unit length, respectively. The index $i \in \{1,2\}$ indicates that the waves at ω_1 and ω_2 are described by the same equations.

Equations (4) and (5) have a well-known solution in terms of the unknown coefficients $\hat{V}_i^+$ and $\hat{V}_i^-$ [12]:

$$\hat{V}_i(x) = \hat{V}_i^+\exp(\gamma x) + \hat{V}_i^-\exp(-\gamma x) \tag{6}$$

$$\hat{I}_i(x) = \frac{-\hat{V}_i^+}{Z}\exp(\gamma x) + \frac{\hat{V}_i^-}{Z}\exp(-\gamma x) \tag{7}$$

Here, $\gamma = \sqrt{(R+j\omega_i L)Y^{(1)}}$ is the propagation constant and $Z = \sqrt{(R+j\omega_i L)/Y^{(1)}}$ is the characteristic impedance. The coefficients are determined by boundary conditions, as described in Section (II-B).

For the waves generated by nonlinear mixing, equation (5) takes its usual form, but Equation (4) must be modified.

$$\begin{aligned} \frac{d\hat{I}_{1+2}}{dx} \approx &-Y^{(1)}(\omega_1+\omega_2)\hat{V}_{1+2} - \\ &2Y^{(2)}(\omega_1,\omega_2)\hat{V}_1\hat{V}_2 \end{aligned} \tag{8}$$

$$\begin{aligned} \frac{d\hat{I}_{1-2}}{dx} \approx &-Y^{(1)}(\omega_1-\omega_2)\hat{V}_{1-2} - \\ &2Y^{(2)}(\omega_1,-\omega_2)\hat{V}_1\hat{V}_2^* \end{aligned} \tag{9}$$

$$\frac{d\hat{I}_{2\times1}}{dx} \approx -Y^{(1)}(2\omega_1)\hat{V}_{2\times1} - Y^{(2)}(\omega_1,\omega_1)\hat{V}_1^2 \tag{10}$$

$$\frac{d\hat{I}_{2\times2}}{dx} \approx -Y^{(1)}(2\omega_2)\hat{V}_{2\times2} - Y^{(2)}(\omega_2,\omega_2)\hat{V}_2^2 \tag{11}$$

Here, the $*$ denotes the complex conjugate, and the factors of 2 in Equations (8) and (9) appear in a straightforward way when we calculate the square of Equation (3).

The key insight of Equations (8-11) is that, because we ignored the nonlinear term when calculating $\hat{V}_1(x)$ and $\hat{V}_2(x)$, we can treat the term proportional to $Y^{(2)}$ as a known function of x. These equations can be solved by a Green's function.

B. Boundary conditions

To determine the coefficients $\hat{V}_i^+$ and $\hat{V}_i^-$, we need to know some relationship between the current and voltage at each end of the transmission line. NVNA's can measure the a and b waves, which are defined in terms of a port impedance $Z_p = 50\ \Omega$ as

$$a \equiv \frac{V + Z_p I}{2} \quad (12)$$

$$b \equiv \frac{V - Z_p I}{2}. \quad (13)$$

We express the a and b waves explicitly in terms of the current and voltage at each end of the transmission line as follows:

$$a_{0,i} = \frac{\hat{V}_i(0) + Z_p \hat{I}_i(0)}{2} \quad (14)$$

$$a_{l,i} = \frac{\hat{V}_i(l) - Z_p \hat{I}_i(l)}{2} \quad (15)$$

$$b_{0,i} = \frac{\hat{V}_i(0) - Z_p \hat{I}_i(0)}{2} \quad (16)$$

$$b_{l,i} = \frac{\hat{V}_i(l) + Z_p \hat{I}_i(l)}{2}. \quad (17)$$

Here, the index i refers to the frequency ω_i, and the subscript 0 refers to the left end of the transmission line, $x = 0$, and the subscript l refers to the right end of the transmission line, $x = l$. The negative sign in Equation (15) and the positive sign in Equation (17) reflect the convention that the a and b waves are defined in terms of the current leaving the test port, whereas $\hat{I}_i(x)$ is the current flowing in the x direction.

As a boundary condition, we assume that the a waves are known at each end of the transmission line at the frequencies ω_1 and ω_2. With some algebra, we can rearrange Equations (14-15), along with Equations (6-7), to solve for the unknown coefficients $\hat{V}_i^+$ and $\hat{V}_i^-$. With some algebra, we can rearrange Equations (14-15), along with Equations (6-7), to find a linear system of equations for $\hat{V}_i^+$ and $\hat{V}_i^-$:

$$\frac{1}{1+\Gamma}\begin{bmatrix} \Gamma & 1 \\ e^{\gamma l} & \Gamma e^{-\gamma l} \end{bmatrix}\begin{bmatrix} \hat{V}_i^+ \\ \hat{V}_i^- \end{bmatrix} = \begin{bmatrix} a_{0,i} \\ a_{l,i} \end{bmatrix}, \quad (18)$$

with the reflection coefficient Γ defined as:

$$\Gamma \equiv \frac{Z - Z_p}{Z + Z_p}. \quad (19)$$

The matrix in Equation (18) can be inverted explicitly:

$$\begin{bmatrix} \hat{V}_i^+ \\ \hat{V}_i^- \end{bmatrix} = \frac{1+\Gamma}{D}\begin{bmatrix} \Gamma e^{-\gamma l} & -1 \\ -e^{\gamma l} & \Gamma \end{bmatrix}\begin{bmatrix} a_{0,i} \\ a_{l,i} \end{bmatrix}, \quad (20)$$

where we have defined the constant

$$D \equiv \Gamma^2 e^{-\gamma l} - e^{\gamma l}. \quad (21)$$

Once we know the coefficients $\hat{V}_i^+$ and $\hat{V}_i^-$, we can calculate $\hat{I}_i(x)$, $\hat{V}_i(x)$ from Equations (6-7). Finally, from the current and voltage, we calculate the outgoing b waves at each port using Equations (16-17). This procedure will faithfully reproduce the linear scattering parameters. We verified this, but don't have space to show it here. Calculating the voltage and current waves at frequencies ω_1 and ω_2 is the first step toward calculating the nonlinear mixing products.

C. Green's Function

The nonlinear wave Equations (8-11) are of the form

$$\frac{d\hat{V}}{dx} = -\left[R(\omega) + j\omega L(\omega)\right]\hat{I} \quad (22)$$

$$\frac{d\hat{I}}{dx} = -Y^{(1)}(\omega)\hat{V} - Y^{(2)}N(x), \quad (23)$$

where $Y^{(2)}N(x)$ is a known function of x that represents the current generated by the nonlinear interaction of the incident waves. These equations can be solved by a Green's function approach [10].

The Green's function approach involves solving for $G_V(x, y)$ and $G_I(x, y)$, the voltage and current waves that are generated by a point current source at a position y along the transmission line. These functions satisfy the differential equations

$$\frac{dG_I(x,y)}{dx} = -Y^{(1)}(\omega)G_V(x,y) + I_0\delta(x-y) \quad (24)$$

$$\frac{dG_V(x,y)}{dx} = -\left[R(\omega) + j\omega L(\omega)\right]G_I(x,y). \quad (25)$$

Here, $\delta(x-y)$ is the Dirac δ function, which models the point-like current source. We include the overall scaling constant I_0 with dimensions of current so that the current Green's function G_I will also have dimensions of current, and G_V will have dimensions of voltage. The value of I_0 is completely arbitrary and has no effect on the end result of this calculation. Once $G_I(x, y)$ and $G_V(x, y)$ are determined, we compute the nonlinear voltage and current by summing the contributions of the currents generated at each position along the transmission line.

$$\hat{V}(x) = -\frac{Y^{(2)}}{I_0}\int_0^l dy G_V(x,y)N(y) \quad (26)$$

$$\hat{I}(x) = -\frac{Y^{(2)}}{I_0}\int_0^l dy G_I(x,y)N(y) \quad (27)$$

We will solve for $G_I(x, y)$ and $G_V(x, y)$ following a very similar procedure to the one we used to solve for $\hat{I}_i(x)$, $\hat{V}_i(x)$ in Section II-B. In addition to the boundary conditions at the ends of the transmission line, the Green's functions satisfy additional boundary conditions at $x = y$. To accommodate these boundary conditions, we write the Green's function in a piecewise form

$$G_V(x,y) = g_V^L(x,y)\Theta(y-x) + g_V^R(x,y)\Theta(x-y) \quad (28)$$

$$G_I(x,y) = g_I^L(x,y)\Theta(y-x) + g_I^R(x,y)\Theta(x-y), \quad (29)$$

where $\Theta(x)$ is the unit step function, and the superscripts R and L stand for "left" and "right". The boundary conditions at $x = y$ are that the voltage is continuous, but the current has a discontinuous jump due to the point current source $I_0\delta(x-y)$.

$$g_I^R(x=y) - g_I^L(x=y) = I_0 \quad (30)$$

$$g_V^R(x=y) - g_V^L(x=y) = 0. \quad (31)$$

Following the same approach we use to solve for $\hat{I}_i(x)$ and $\hat{V}_i(x)$ in section II-B, we will express the Green's function in terms of unknown coefficients.

$$g_V^L(x,y) = g_L^+(y)\exp(\gamma x) + g_L^-(y)\exp(-\gamma x) \quad (32)$$

$$g_V^R(x,y) = g_R^+(y)\exp(\gamma x) + g_R^-(y)\exp(-\gamma x) \quad (33)$$

$$g_I^L(x,y) = -\frac{g_L^+(y)}{Z}\exp(\gamma x) + \frac{g_L^-(y)}{Z}\exp(-\gamma x) \quad (34)$$

$$g_I^R(x,y) = -\frac{g_R^+(y)}{Z}\exp(\gamma x) + \frac{g_R^-(y)}{Z}\exp(-\gamma x) \quad (35)$$

The boundary conditions will lead to a matrix equation for the unknown coefficients.

$$\begin{bmatrix} \Gamma & 1 & 0 & 0 \\ 0 & 0 & e^{\gamma l} & \Gamma e^{-\gamma l} \\ -e^{\gamma y} & -e^{-\gamma y} & e^{\gamma y} & e^{-\gamma y} \\ -e^{\gamma y} & e^{-\gamma y} & e^{\gamma y} & -e^{-\gamma y} \end{bmatrix} \begin{bmatrix} g_L^+(y) \\ g_L^-(y) \\ g_R^+(y) \\ g_R^-(y) \end{bmatrix} = \begin{bmatrix} 0 \\ 0 \\ 0 \\ ZI_0 \end{bmatrix} \quad (36)$$

Equation (36) admits a closed form solution, which we found by standard techniques [10].

$$g_L^+(y) = \left(\frac{ZI_0}{2D}\right)\left[\Gamma e^{\gamma(y-l)} - e^{-\gamma(y-l)}\right] \quad (37)$$

$$g_L^-(y) = \left(\frac{ZI_0}{2D}\right)\left[-\Gamma^2 e^{\gamma(y-l)} + \Gamma e^{-\gamma(y-l)}\right] \quad (38)$$

$$g_R^+(y) = \left(\frac{ZI_0}{2D}\right)\left[\Gamma e^{\gamma(y-l)} - \Gamma^2 e^{-\gamma(y+l)}\right] \quad (39)$$

$$g_R^-(y) = \left(\frac{ZI_0}{2D}\right)\left[-e^{\gamma(y+l)} + \Gamma e^{-\gamma(y-l)}\right] \quad (40)$$

D. Overview

In summary, here is a recipe to predict the 2nd-order mixing products generated a transmission line with a nonlinear distributed capacitance.

1) For each incident frequency ω_i, we use Equation (20) to solve for the coefficients $\hat{V}_i^+$ and $\hat{V}_i^-$ from the measured a waves at the edges of the transmission line.
2) From $\hat{V}_i(x)$, we compute the nonlinear driving term, $N(y)$, for each mixing frequency of interest.
3) We compute the voltage and current Greens functions, given by Equations (28-29), (32-35), and (37-40).
4) We then use Equations (26-27) to determine the spatial distribution of voltages and currents generated by nonlinear mixing.
5) Using boundary conditions given in Equations (16-17), we can compute the outgoing b waves at the reference planes of the edge of the transmission line.

III. Sample Preparation and Linear Measurements

Figure 2a shows the cross section of our nonlinear transmission lines, as designed. We lithographically fabricated transmission lines on a nonlinear BST film. The film was 1 µm thick and was deposited by pulsed laser deposition on a $LaAlO_3$ substrate. The transmission lines were gold coplanar waveguides, with 200 µm ground planes, a nominal 20 µm center conductor, 5 µm gaps, and 500 nm metalization thickness.

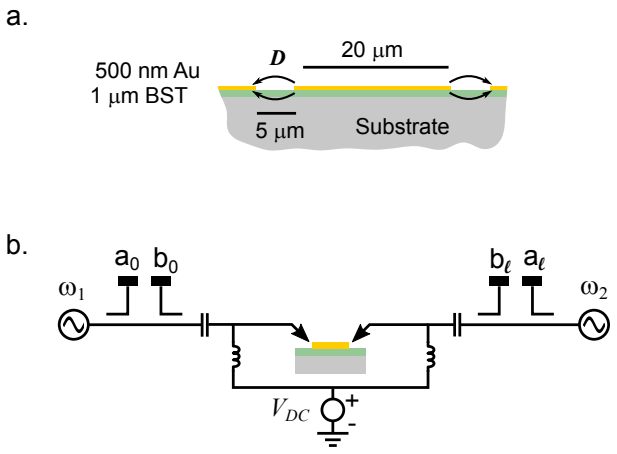

Fig. 2: Experimental configuration. a) Nonlinear transmission line cross section geometry with design dimensions. b) Measurement configuration. Both ends of the waveguide were excited simultaneously, and the a and b waves at ω_1, ω_2 and $\omega_1 + \omega_2$ were recorded.

To determine the linear circuit parameters necessary for the model (Figure 1b), we measured the scattering parameters of each of the transmission lines. These measurements were error-corrected by an on-wafer multiline TRL calibration [13] on a lossless, linear substrate. To get the distributed admittance $Y^{(1)}$, we performed a 2nd-tier multiline TRL calibration on the transmission lines fabricated on the BST chip to extract the propagation constant, γ. Finally, we computed the distributed resistance R and inductance L using a finite-element method [14]. From γ, R, and L, we were able to determine the distributed admittance.

IV. Nonlinear Measurements

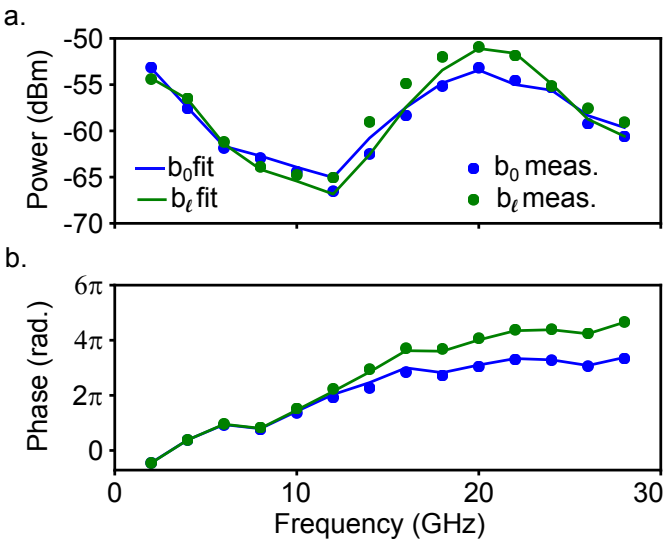

Fig. 3: Nonlinear measurements of the outgoing b wave at $\omega_1 + \omega_2$, with $\omega_1/2\pi$ = 1 GHz. a) Power, de-embedded to on-wafer reference plane. b) Unwrapped phase at on-wafer reference plane.

We performed "proof of concept" measurements with an NVNA (Figure 1.b). We found that our sample has no 2nd-order nonlinearity unless it is poled by an external electric field, so we applied a 10 V DC bias between the center conductor and ground planes of the CPW line. The transmission line, with a length of $l = 535$ μm, was excited by signals with a source power of 0 dBm. On the left port (port 0), we applied a tone with a fixed frequency of $\omega_1/2\pi$ = 1 GHz. On the right port (port l), we varied the frequency from $\omega_2/2\pi$ = 2 GHz to $\omega_2/2\pi$ = 28 GHz. The ports are denoted 0 and l, because the left and right ends of the transmission line are denoted by $x = 0$ and $x = l$, and because subscripts 1 and 2 refer to frequencies ω_1 and ω_2 throughout this paper.

We corrected these measurements using a two-tier calibration, as described in the manual for the NIST Uncertainty Framework software [15]. First, we performed a coaxial SOLT calibration, as well as phase and power calibrations to the coaxial reference plane. Then, we attached the coaxial cables to microwave probes and performed an on-wafer series resistor calibration. The two-tier calibration was necessary because on-wafer phase and power standards are not available. The on-wafer calibration allows us to roll the reference planes to an on-wafer reference plane (the edge of the series resistor).

Figure 3 shows the corrected b wave, at the on-wafer reference plane, for the wave at $\omega_1+\omega_2$. We show both b_0 and b_l, the waves measured at the left side of the transmission line ($x = 0$) and the right side of the transmission line ($x = l$). b_0 and b_l have similar, but non-identical frequency dependence; the amplitude and phase of these waves depends on frequency, because of distributed effects. There is no symmetry in this problem demanding that b_0 and b_l be identical, and in a longer line, they may be very different. In this particular case, the phases are very similar below 10 GHz because the transmission line is relatively short and one of the waves is at 1 GHz. The nonlinear mixing products shown in this section are due to the nonlinearity of our BST sample, not the sources or the receivers in the NVNA. We verified this by performing identical measurements on transmission lines with an identical cross section on a linear material ($LaAlO_3$).

According to Equations (26) and (27), the b nonlinear signal at $\omega_1 + \omega_2$ is proportional to $Y^{(2)}(\omega_1, \omega_2)$. So, we can compute $Y^{(2)}(\omega_1, \omega_2)$ in a straightforward way from these measurements. We take the measured a waves at each port for all frequencies as known, and compute the b waves as described in Section (II-D). Then, the nonlinear admittance can be computed as,

$$Y^{(2)}(\omega_1, \omega_2) = \frac{b_{obs}}{b_{NL}}, \tag{41}$$

where b_{NL} is the nonlinear calculated wave with an assumed value of $Y^{(2)} = 1$, and b_{obs} is the observed wave. In the calculations shown in Figure 3, the only fit parameter is $Y^{(2)}$. We determined the value of $Y^{(2)}$ by applying Equation (41) to the measured values of b_0 and b_l to obtain two estimates of $Y^{(2)}$, and averaging these two estimates. In this data set, the magnitude of these two estimates agrees at all frequencies, but their phase only agrees below 10 GHz.

By repeating measurements of the b waves on many different transmission lines of differing lengths, we can infer 2 independent measurements of $Y^{(2)}$ from each line corresponding to the 2 ends of the line. By performing measurements on several lines, we plan to both test the model and determine a better estimate of $Y^{(2)}$.

V. Conclusion

These measurements demonstrate that we can measure the amplitude and phase of 2nd-order mixing products by NVNA. We have strong evidence for the validity of our analytic solution of the nonlinear wave equations, and are in the process of building confidence by performing more measurements. The mathematical formulation and proof-of-concept measurements presented here pave the way for on-wafer nonlinear dielectric characterization. As we described in Section (IV), we can infer the strength of the nonlinearity from these measurements. We expect that $Y^{(2)}$ and $\varepsilon^{(2)}$ are directly related, and that we will be able to quantify this relationship with element simulations.

References

[1] E. G. Erker, A. S. Nagra, Y. Liu, P. Periaswamy, T. R. Taylor, J. Speck, and R. A. York, "Monolithic ka-band phase shifter using voltage tunable BaSrTiO3 parallel plate capacitors," *IEEE Microwave and Guided Wave Letters*, vol. 10, no. 1, pp. 10–12.

[2] X. Wang, J. Ren, and R. J. Hwu, "Millimeter-wave nonlinear transmission line tripler," vol. 3465. International Society for Optics and Photonics, pp. 98–104.

[3] Y. E. Wang, "Time-varying transmission lines (TVTL) - a new pathway to non-reciprocal and intelligent RF front-ends," in *2014 IEEE Radio and Wireless Symposium (RWS)*, pp. 148–150.

[4] A. K. Tagantsev, V. O. Sherman, K. F. Astafiev, J. Venkatesh, and N. Setter, "Ferroelectric materials for microwave tunable applications," *Journal of Electroceramics*, vol. 11, no. 1, pp. 5–66.

[5] J. C. Booth, I. Takeuchi, and K.-S. Chang, "Microwave-frequency loss and dispersion in ferroelectric $Ba_{0.3}Sr_{0.7}TiO_3$ thin films," *Applied Physics Letters*, vol. 87, no. 8, p. 082908.

[6] C.-H. Lee, N. D. Orloff, T. Birol, Y. Zhu, V. Goian, E. Rocas, R. Haislmaier, E. Vlahos, J. A. Mundy, L. F. Kourkoutis, Y. Nie, M. D. Biegalski, J. Zhang, M. Bernhagen, N. A. Benedek, Y. Kim, J. D. Brock, R. Uecker, X. X. Xi, V. Gopalan, D. Nuzhnyy, S. Kamba, D. A. Muller, I. Takeuchi, J. C. Booth, C. J. Fennie, and D. G. Schlom, "Exploiting dimensionality and defect mitigation to create tunable microwave dielectrics," *Nature; London*, vol. 502, no. 7472, pp. 532–6.

[7] A. E. Glazounov and A. K. Tagantsev, "Phenomenological model of dynamic nonlinear response of relaxor ferroelectrics," *Physical Review Letters*, vol. 85, no. 10, pp. 2192–2195.

[8] J. Mateu, C. Collado, N. Orloff, J. C. Booth, E. Rocas, A. Padilla, and J. M. O'Callaghan, "Third-order intermodulation distortion and harmonic generation in mismatched weakly nonlinear transmission lines," *IEEE Transactions on Microwave Theory and Techniques*, vol. 57, no. 1, pp. 10–18.

[9] J. Mateu, J. C. Booth, and S. A. Schima, "Frequency tuning and spurious signal generation at microwave frequencies in ferroelectric SrTiO3 thin-film transmission lines," *IEEE Transactions on Microwave Theory and Techniques*, vol. 55, no. 2, pp. 391–396.

[10] I. Stakgold and M. J. Holst, *Green's Functions and Boundary Value Problems*. John Wiley & Sons.

[11] M. Neshat, D. Saeedkia, and S. Safavi-Naeini, "Semi-analytical calculation of terahertz signal generated from photocurrent radiation in traveling-wave photonic mixers," *International Journal of Infrared and Millimeter Waves*, vol. 29, no. 9, pp. 809–822. [Online]. Available: https://link.springer.com/article/10.1007/s10762-008-9388-z

[12] D. M. Pozar, *Microwave Engineering*, 4th ed. Wiley.

[13] R. B. Marks, "A multiline method of network analyzer calibration," *IEEE Transactions on Microwave Theory and Techniques*, vol. 39, no. 7, pp. 1205–1215.
[14] W. T. Weeks, L. L. H. Wu, M. F. McAllister, and A. Singh, "Resistive and inductive skin effect in rectangular conductors," *IBM Journal of Research and Development*, vol. 23, no. 6, pp. 652–660.
[15] D. Williams and A. Lewandowski, "NIST microwave uncertainty framework," *National Institute of Standards and Technology*, 2011.